9 February 1968, Volume 159, Number 3815 **SCIENCE**

Molecular Beams and a Chemical Reaction

Results for the reaction of potassium with methyl iodide show how beam experiments and theoretical work contribute to chemical kinetics.

E. F. Greene and J. Ross

In the 13 years that have passed since the first successful studies of chemical reactions with molecular beams (*1*), many people have applied these methods to learn how reactions occur. Here we illustrate the progress in this field by selecting one bimolecular reaction, that of potassium atoms with methyl iodide molecules, and by describing for it the experiments done, the analysis of these experiments, and some of the theoretical work which helps us understand them. Several longer reviews are available (*2–4*).

Distributions

Let us consider what happens in the more usual ways of studying reactions in gases. In a gas, which may be pure or a mixture of different chemical species, at thermal equilibrium at a temperature T and at a low pressure, the molecules are far enough apart to be nearly independent. They interact only during the small fraction of the time when pairs of them collide. Collisions involving three or more molecules are negligible. The motions of the molecules are random, subject to the restriction that the total energy remains constant. As a result of collisions, not only the directions and speeds but also the rotational and vibrational motion of individual molecules in the collection change with time. As a good approximation we divide E_{tot} (the total energy of the molecules) into parts corresponding to energies of translation, rotation, vibration, and electronic excitation as follows,

$$E_{\text{tot}} = E_{\text{trans}} + E_{\text{rot}} + E_{\text{vib}} + E_{\text{el}} \tag{1}$$

Solid lines in Fig. 1, c, e, f, and g show, for our model reaction, the distribution at equilibrium of the separate reactant molecules over the range of possible values for each kind of energy. We choose potassium at 405°C and CH_3I at 15°C because these temperatures are near those used for molecular-beam experiments described below. The translational quantum levels are close enough together in energy to be drawn as a continuous distribution; the rotational, vibrational, and electronic levels are spaced successively further apart. Many excited rotational states of CH_3I are populated, but relatively few molecules are above the lowest vibrational state, and essentially all of both K and CH_3I are in their ground electronic states.

Polanyi and his collaborators have made the most significant studies of reactions similar to those of the alkali metals with methyl iodide, for which the reactants were distributed thermally (*5*). For example, von Hartel and Polanyi (*6*) followed the reaction

$$Na + CH_3I \longrightarrow NaI + CH_3 \tag{2}$$

by allowing Na at 250°C and 10^{-3} torr to diffuse into CH_3I, while they monitored the Na concentration in the "flame" by its scattering of the resonance radiation from a sodium vapor lamp. They estimated that reaction occurred "roughly . . . at every collision" between Na and CH_3I, so the activation energy had to be nearly zero.

Reactions in Molecular Beams

Molecules in beams do not have to have these thermal distributions, but may be selected, at least in principle, so that each beam consists of molecules in only one quantum state or perhaps a small range of states (which we label i and j for the two reactants). In addition, when reactions occur, the relative speed v and the relative orientation γ between the molecules in the two beams can be selected, and the states in which the products are formed can be determined. For our reaction this can be represented by the stoichiometric equations

$$\xrightarrow{\text{elastic}} K\,(i) + CH_3I(j) \tag{3a}$$

$$K(i)+CH_3I(j) \xrightarrow{v,\,\gamma\quad\text{inelastic}} K\,(k) + CH_3I(l) \tag{3b}$$

$$\xrightarrow{\text{reactive}} KI(m) + CH_3(n) \tag{3c}$$

In elastic scattering (Eq. 3a), there is no change in the quantum states of the colliding molecules or in the speed of relative motion v, although the direction of their relative motion does change. Inelastic processes like the conversion of translational to vibrational energy lead to changes of quantum states but not of chemical species (Eq. 3b); reactive collisions produce new kinds of molecules (Eq. 3c). Here one subscript represents all the quantum numbers needed to characterize the internal state for that molecule. All three kinds of scattering show something about

---

Dr. Greene is professor of chemistry at Brown University, Providence, Rhode Island 02912, and was a National Science Foundation senior postdoctoral fellow at the California Institute of Technology during 1966–67; Dr. Ross is professor of chemistry at the Massachusetts Institute of Technology, Cambridge 02139.

how the molecules interact and help us to determine the criteria for reaction.

The dashed curves in Fig. 1 show to what extent selection has narrowed the ranges of states for K and CH_3I in some molecular-beam experiments. As yet no real experiment can give the perfect selection indicated by Eq. 3, but many details of chemical reactions are becoming clearer through partial selection.

We can ask two kinds of questions about experiments: (i) What can this experiment tell us directly, what is the measurable quantity? (ii) What can we deduce from the results?

For molecular-beam experiments, examples of the first kind of question are: (i) What is the chance for a K atom and a CH_3I molecule to interact at all as they pass each other, or what is the total cross section $Q(v)$ (commonly given in units of square angstroms per molecule) at a particular relative speed, and how does this vary with relative speed or energy? (ii) What chance is there of scattering to a particular solid angle ω, or what is the differential cross section $\sigma(v\omega)$ (commonly given in units of square angstroms per molecule per steradian), and how does it vary with energy? (iii) In what internal energy states are the products formed, and with what speed do they separate after the reaction? (iv) What is the chance for reaction at a given relative speed, or what is the total reaction cross section $Q_R(v)$? What is the threshold energy, and what is the variation of the total reaction cross section with energy? (v) How does the inelastic and reactive scattering depend on the initial relative orientation of the colliding molecules?

We now show how some of these answers to the first kind of questions are found and how they in turn help to answer some questions of the second kind, such as: (i) Is a collision complex formed; and, if so, what is its lifetime? (ii) What is the relation of the interactions and the scattering to the electronic and geometric structure of the reactants?

Important features of the necessary apparatus are: beam sources—usually small boxes of gas from which molecules escape through a small hole; collimating slits to reject all molecules moving in unwanted directions; a velocity selector to reject all molecules moving with unwanted speeds; an orientation selector to reject molecules of unwanted orientation; a scattering region where the two beams cross and the molecules can interact; and finally a movable detector to record the number of molecules of reactants or products which are scattered to a particular angle (Fig. 2). We omit both a velocity analyzer to measure the speed of the products and any device to determine the rotational state of the products

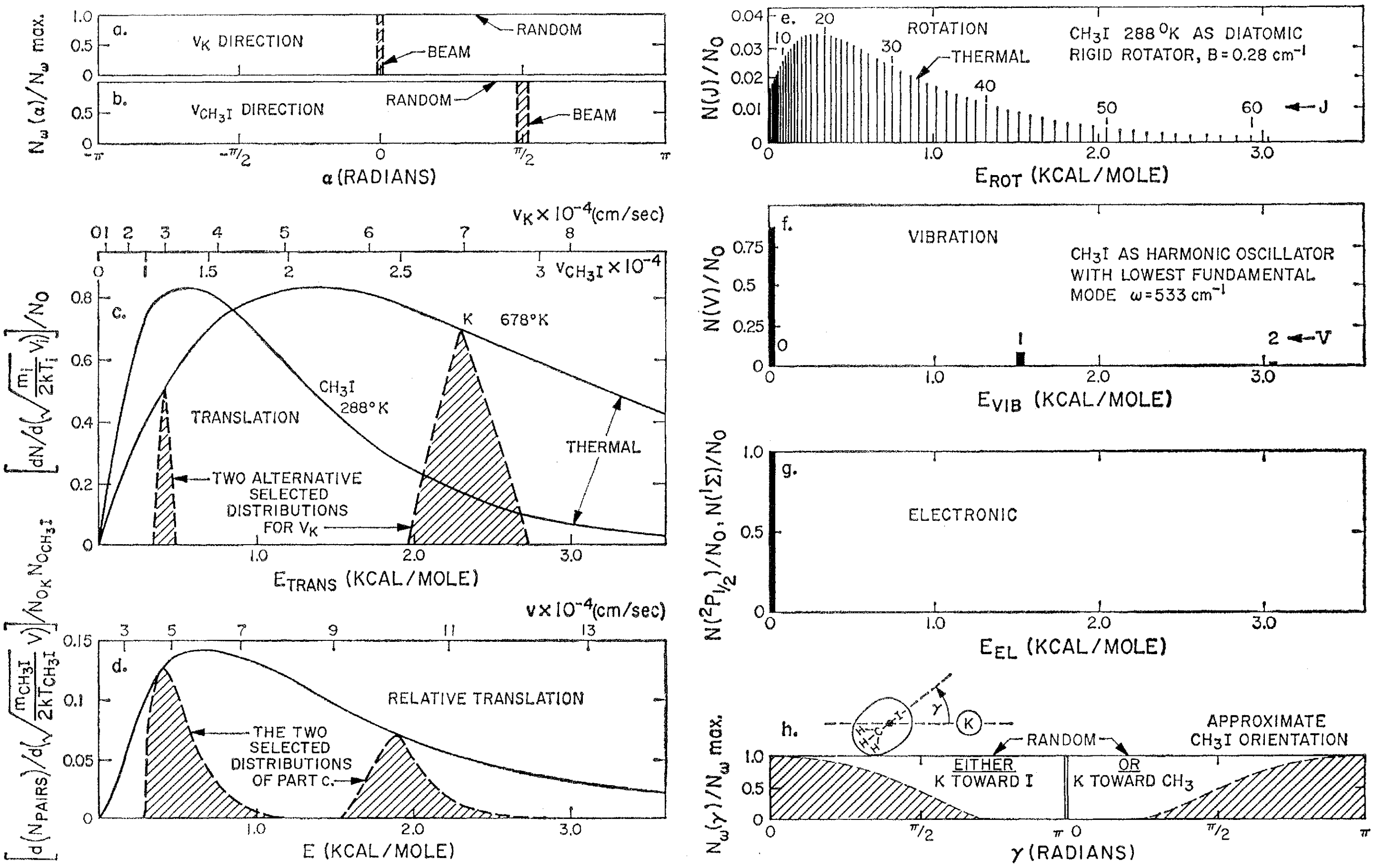

Fig. 1. Distributions of direction and energy for K and CH_3I. Solid lines for thermal equilibrium, K, 405°C; CH_3I, 15°C. Dashed lines enclose shaded area to indicate distribution after selection for a molecular-beam experiment. The symbol $N(i)$ indicates the number of molecules in state i; N_ω is the number per unit solid angle; N_0 is the total number of molecules, E_n is the energy of the n_{th} kind. (a) Direction of K velocity in laboratory. (b) Direction of CH_3I velocity in laboratory. (c) Translational energies of K and CH_3I; the corresponding speeds v_i for $i = K$, CH_3I are also shown. (d) Translational energy of relative motion for a pair of molecules K–CH_3I. The relative speed v is shown also. (e) Rotational energy of CH_3I approximated as a rigid, diatomic molecule with rotational constant $B = 0.28$ cm⁻¹. The rotational quantum numbers J are shown. (f) Vibrational energy of CH_3I for the lowest fundamental mode (533 cm⁻¹) taken as a harmonic oscillator. The vibrational quantum numbers V are shown. (g) Electronic energy for K and CH_3I. Only the ground states are appreciably populated. (h) Orientation angle γ of CH_3I with respect to the relative velocity of K and CH_3I before the collision.

because results based on these parts of a more complete apparatus have not yet been reported for the reaction of K with CH_3I. Each of these selection processes works essentially by rejecting unwanted molecules and hence reduces the number of molecules in the beam. Thus in each actual experiment one or more of these parts had to be omitted to avoid reducing the intensity of scattered molecules so much that this signal would disappear in the background of noise. In each diagram giving the experimental results the inserts show the components of Fig. 2 used for that experiment.

Total Scattering Cross Section

To measure the effective size of the molecules we ask for the chance of any scattering at all. In principle, for the apparatus shown in Fig. 2 we would set the detector at α equal to 0, adjust the velocity selector to give K atoms of a particular speed (v_K), and record the flux of K at the detector in the presence [$N_K(v)$] and absence [$N_K{}^{\circ}(v)$] of CH_3I in the cross beam. For beams intersecting at 90°, the relative speed v is

$$(v_K{}^2 + v_{CH_3I}{}^2)^{\frac{1}{2}}$$

For a representative speed of the CH_3I molecules in the beam we might use, as an approximation, the most probable speed of CH_3I in the oven $(2\ RT/m_{CH_3I})^{1/2}$, where R is the gas constant, T the CH_3I oven temperature, and m_{CH_3I} the mass of CH_3I. The corresponding relative kinetic energy E is $\frac{1}{2}\ \mu v^2$; the reduced mass μ is $m_K m_{CH_3I}/(m_K + m_{CH_3I})$. For comparison with Eq. 1 we have the relation

$$E_{\mathrm{trans,\ K}} + E_{\mathrm{trans,\ CH_3I}} = E + E_{cm}$$

E is the important variable, the energy of relative motion, while E_{cm}, the energy of motion of the center of mass, is constant for the collision.

The total cross section [$Q(v)$] is defined by Eq. 4:

$$N_K(v) = N_K{}^{\circ}(v)\exp\left[-Q(v)n_{CH_3I}vl\right] \quad (4)$$

Here n_{CH_3I} is the density of CH_3I molecules averaged over the length l of the region where the two beams cross and scattering would occur.

Although no one has yet done this experiment, we can make an estimate of $Q(v)$ as follows. Rothe and Bernstein (*7*) have measured $Q(\bar{v})_{\mathrm{K-CH_3I}}/Q(\bar{v})_{\mathrm{K-Ar}}$, and Rothe and Neynaber (*8*) have reported an absolute value for $Q(\bar{v})_{\mathrm{K-Ar}}$. Here $\bar{v}$ is the average relative speed in these experiments (*7, 8*) which were done with thermal beams of K atoms passing through a chamber containing either CH_3I or Ar. The cross in Fig. 3 indicates the resulting value of $Q(\bar{v} = 655\ \mathrm{m/sec})_{\mathrm{K-CH_3I}}$. The triangles in the figure show the speed dependence $Q(v)$ measured by Gislason and Kwei (*9*) for the similar system Na–CH_3I normalized to $Q(\bar{v})_{\mathrm{K-CH_3I}}$. Figure 3 shows that for a relative speed of 655 m/sec the effective area presented to a K atom by a CH_3I molecule may be expected to be about 10×10^2 Å^2. To interpret this result we assume that the energy of interaction [$V(r)$] is independent of the orientation of the CH_3I, and also that, despite the possibility of chemical reaction, this energy varies with the distance of separation r, for large r, as given by the Lennard-Jones potential

$$V(r) = \epsilon\left[(r_m/r)^{12} - 2(r_m/r)^6\right]. \quad (5)$$

The parameters ϵ and r_m are defined in Fig. 4a. For low kinetic energies ($E \tilde{<} \epsilon$) the total cross section $Q(v)$ is determined almost entirely by the attractive part of the potential, the second term in Eq. 5. The coefficient of r^{-6} in this term, $2\epsilon r_m{}^6$, is related (*10*) to the total cross section by

$$Q(v) = 8.083\ (2\epsilon r_m{}^6/\hbar v)^{\frac{2}{5}} \quad (6)$$

where $\hbar$ is Planck's constant over 2π and both the values of the factor 8.083 and the exponent ⅖ depend on the exponent 6 in the second term of Eq. 5. Thus the agreement of the slope of the experimental points in Fig. 3 with the value of ⅖ required by Eq. 6 confirms that the interaction energy between Na and CH_3I, and presumably also K and CH_3I, does vary as r^{-6} at large r as expected theoretically (*11*). Further, the magnitude of $Q(v)$ gives us a value for the product $\epsilon r_m{}^6$ equal to 6.4×10^{-58} erg cm^6. Thus, a measurement of the total cross section tells about the nonreactive interaction of the two molecules at large distances.

Elastic Scattering

We learn more about the interaction of K with CH_3I by measuring how much K is scattered by CH_3I to a particular laboratory angle α for a given relative speed v, or relative kinetic energy E (differential scattering cross section) (*12*). These experiments could not distinguish between elastically and inelastically scattered K (Eqs. 3a and 3b), and we assume here that the latter is insignificant in comparison to the former (Fig. 5a). In Fig. 5b we have replotted the same points reduced as suggested by Smith, Marchi, and Dedrick (*13*). Here θ, the scattering angle in center-of-mass coordinates, is $c\alpha$. The quantity c is nearly constant; it varies only from 1.26 to 1.18 as α varies from 2° to 70°; θ is defined in Fig. 9b. The structure of Fig. 5a is emphasized by the way of plotting Fig. 5b, and the points for the two energies fall on almost exactly the same reduced curve. The maximum which comes near $E\theta$ equal to 50 (degrees kilocalories per mole) in Fig. 5b is due to an increased probability of scattering near an angle θ_r called

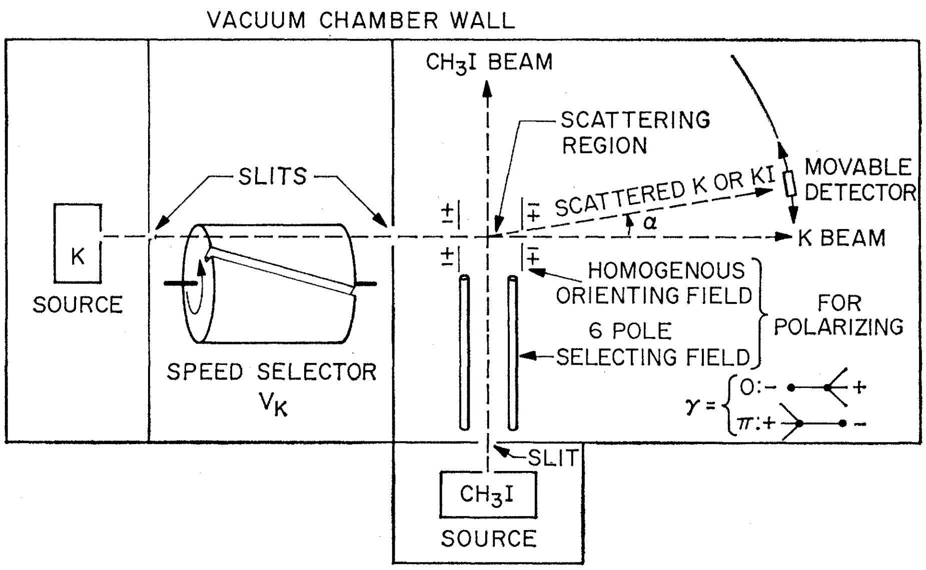

Fig. 2. Diagram of a molecular beam apparatus to study the reaction of K with CH_3I. For the two field polaries the CH_3I tends to be oriented in a range near zero or π.

the rainbow angle. (The name calls attention to the similarity between this scattering and that which produces rainbows in the sky.) The physical reason for the presence of the maximum is seen by considering the trajectories drawn in Fig. 4b. Each of the lines with arrowheads represents the change with time of the distance between two particles originally approaching each other at a fixed relative speed v. The lines are trajectories in relative coordinates. Each represents a collision with a different impact parameter or amount of off-centerness b (the displacement of the trajectory at large values of r from a line parallel to it through the origin) or the corresponding angular momentum μvb. These trajectories are calculated according to classical mechanics for two particles which interact with a potential energy given by Eq. 5 or Fig. 4a. For large values of b the attractive forces predominate, and the trajectory is pulled toward the scattering center. By definition this is a negative deflection. As the value of b decreases, the deflection first becomes increasingly negative until, at the rainbow angle,

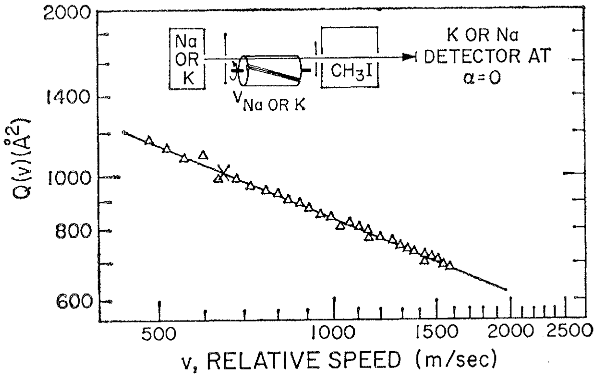

Fig. 3. Total cross section $Q(v)$ plotted against the relative speed v estimated for K–CH_3I from: (×) value of Q for average speed of thermal K beam scattered from CH_3I in a scattering chamber (7, 8); (Δ) $Q(v)$ for NA–CH_3I(9) normalized to (×). Solid line: slope calculated for potential varying as r^{-6} at large values of r.

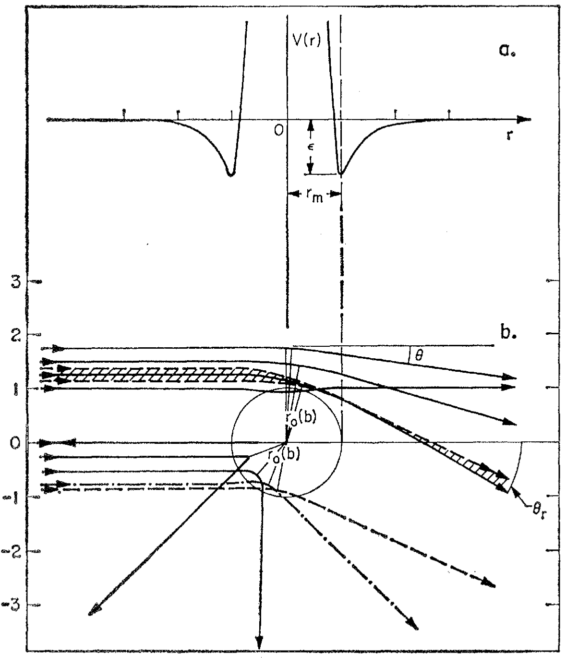

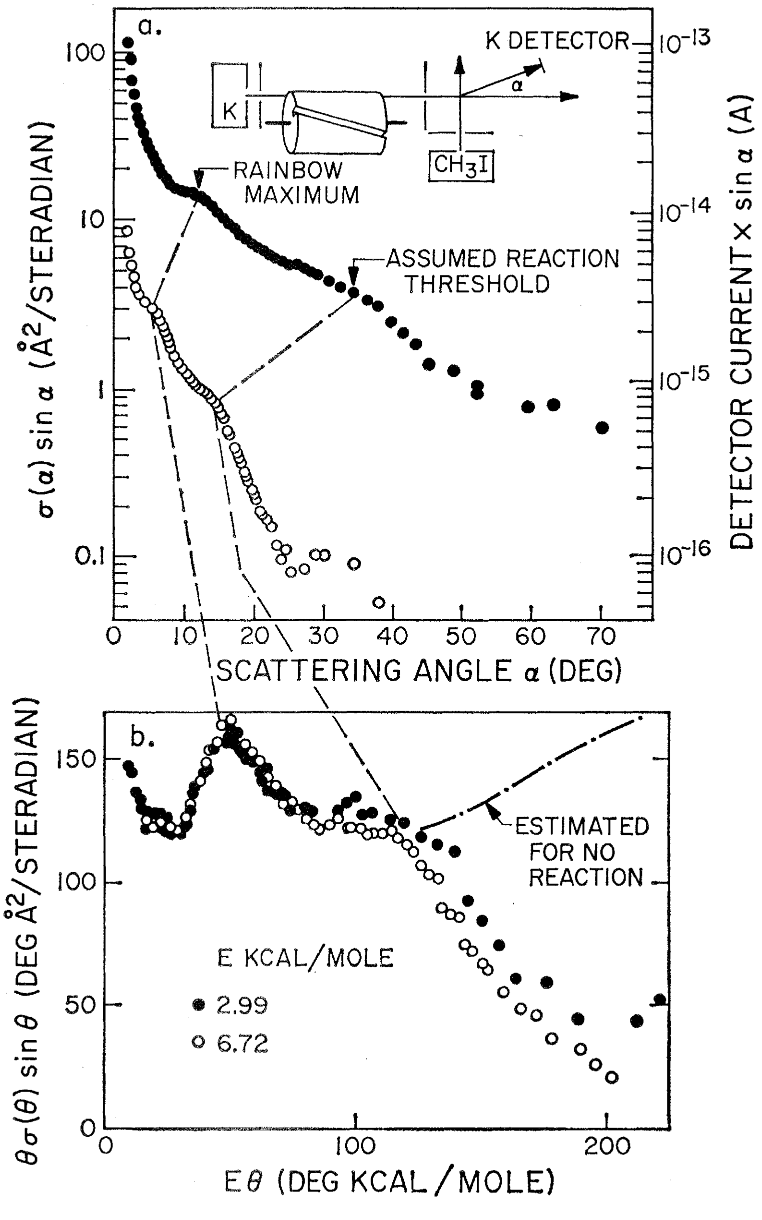

Fig. 4 (left). (a) Lennard-Jones potential for the interaction of two spherically symmetrical particles, Eq. 5. (b) Trajectories calculated for particles interacting according to Eq. 5 for one relative kinetic energy and several values of the impact parameter b. For each b there is a corresponding distance of closest approach r_0 and deflection angle θ. Trajectories with three different values of b, the dashed lines for example, contribute to scattering for $\theta < \theta_r$, the rainbow angle. The dot-dashed curve with $\theta > \theta_r$ is the only trajectory for its θ. A corresponding set of trajectories, omitted here, is obtained by reflecting these in the line for $b = 0$. This other set would give upward deflections. Fig. 5 (right). (a) Differential cross section times sin α for the scattering of K by CH_3I to laboratory angle α for two initial relative kinetic energies E. For clarity the points for $E = 6.72$ kcal/mole are plotted at 0.1 of their proper values. The absolute values of the cross section and the detector current are only approximate, but they show the magnitudes involved. (b) Reduced differential cross section for scattering of K by CH_3I to center-of-mass angle θ plotted against E for the same energies. The dashed lines connect corresponding regions on the various curves. The dot-dash line is our estimate of the scattering expected in the absence of reaction.

it reaches its nadir, and then becomes progressively more positive as the repulsive forces become dominant. For head-on collisions ($b = 0$), the trajectory returns on itself with a deflection of 180°. The colliding molecules come increasingly close together as b approaches zero. The distance of closest approach for one trajectory is $r_o(b)$. The trajectories are not directed uniformly to all angles, but are concentrated at angles just less than the rainbow angle. This accumulation of trajectories produces the corresponding rainbow maximum. For example, in Fig. 4b, which shows a set of trajectories, each of the three dashed curves (two representing negative deflections and one a positive one) would be detected at the same angle in an experiment, whereas only one curve (with a positive deflection, for example the dot-dashed curve) corresponds to a particular θ if it is greater than θ_r. The deflection at the rainbow angle increases as the depth of the potential well increases, and it decreases as the relative speed v increases. A higher v means a faster passage and consequently less time for the forces to produce a deflection. In practice θ_r is very nearly proportional to ϵ/E. Thus by setting our velocity selector for a known v we find E ($= \frac{1}{2}\ \mu\ v^2$), and by locating the rainbow angle on the differential cross section (Fig. 5) we find ϵ/E. The product gives ϵ directly; its value is 0.51 kilocalories per mole or 3.5×10^{-14} erg per molecule. This value of ϵ and that of $\epsilon r_m{}^6$ from the total cross section allow us to calculate $r_m = (\epsilon r_m{}^6/\epsilon)^{\frac{1}{6}} = 5.0$ Å. This is only one of several procedures used, and it gives us a quantitative (although certainly not unique) description of the interaction of K and CH_3I for nonreactive collisions, once we have assumed the form given by Eq. 5.

Another feature of the differential cross section plotted in Fig. 5 is the sharp drop, which is particularly visible in Fig. 5b near $E\theta = 120$. There is a shortage of K atoms scattered by CH_3I to large angles, compared to those scattered by nonreactive molecules. This apparently represents a loss of K because, for some of the trajectories leading to these larger scattering angles, reaction is taking place, and it removes the K by forming KI. The dot-dashed curve in Fig. 5b is our guess for the position of the hypothetical curve for no reaction suggested by the study of nonreactive systems.

Now we use a very simple idea (*14*) to try to learn about the reaction from these measurements of the scattered K. At any angle $E\theta$ greater than that, $E\theta_{\text{th}}$, at which the dot-dashed and CH_3I curves separate, we assume that the ordinate of the dot-dashed curve $\theta\sigma_o \sin\theta$ gives the amount of K which would have appeared if reaction had not occurred, while the ordinate for the CH_3I curve, $\theta\sigma_{CH_3I} \sin\theta$, gives the amount of K observed. Thus for each angle we can estimate the probability of reaction P from

$$P(\theta) = (\sigma_o - \sigma_{CH_3I})/\sigma_o \qquad (7)$$

Moreover, for any angle θ we can immediately find the corresponding values of b and r_o if we have already determined v, E^{ϵ}, and r_m. The latter two quantities come from the scattering measurements and the assumed form of Eq. 5; v comes from the setting of the velocity selector. Thus we can plot the variation of P with b and $r_o(b)$ or $V(r_o)$ as in Fig. 6. It is interesting that the probability has threshold values at $b_{\text{th}} = 4.2$ Å and $V(r_o)_{\text{th}} = 0.3 \pm 0.2$ kcal/mole. We can compare this value for $(r_o)_{\text{th}} = 4.1$ Å, the largest r_o for which reaction is possible with an estimate based on a highly simplified model (*12*). Let us suppose that the threshold occurs at the largest r_o for which the formation of KI is energetically possible. This is the r_o at which all the relative kinetic energy of the reactants plus the energy liberated in the reaction becomes internal energy of the product KI. To this diatomic molecule we assign a potential energy curve representing the energy of the system as a function of the internuclear distance. We give the KI this maximum internal energy and then take for r_o the largest classically allowed internuclear distance. From the equilibrium internuclear distance of KI (3.05 Å) and the Morse potential we estimate the threshold distance to be 4.14 Å, in perhaps surprising agreement with $(r_o)_{\text{th}}$.

We can make further use of the nonreactive scattering measurements by estimating the total reaction cross section $Q_R(v)$. To do this we add up all the missing K signal in Fig. 5 by integrating over b or θ to get the total reaction cross section,

$$Q_R(v) = 2\pi \int_0^{b_{\text{th}}} Pb\, db = 2\pi \int_{\theta_{\text{th}}}^{\pi} P\sigma_o \sin\theta\, d\theta \qquad (8)$$

The variation of $Q_R(v)$ with energy is plotted in Fig. 7.

A rough comparison with the results of von Hartel and Polanyi (*6*) is possible. Their reaction "at every collision" for hard spheres is entirely consistent with a reaction cross section like the one in Fig. 7.

Reactive Scattering

An important way to learn about the reaction of K with CH_3I is to find the yield of products, KI or CH_3, directly. Herschbach, Kwei, and Norris (*15*) did just this by measuring the angular distribution of KI formed when beams of K and CH_3I, effusing from ovens at fixed temperatures, crossed at a known angle (*16*). This was the first molecular-beam experiment with this reaction. In Fig. 8 we plot their results (*17*) for a 90° angle of intersection and the oven temperatures which characterize the distributions of Fig. 1. Thus the ranges of E_{trans}, E, E_{rot}, E_{vib}, E_{el}, and γ for K and CH_3I are those shown by solid lines in Fig. 1. The rainbow maximum and reaction threshold visible in Fig. 5, for which the K beams were velocity selected, are hidden in Fig. 8 because of the wider range of the thermal distribution of speeds. The useful contribution of molecular beams here is to reduce the range of angles of intersection and to permit the observation of the products from one collision before a second occurs. In comparison with the thermal reaction, even this simple beam experiment produces a striking clarification of the nature of the reaction. We show the essential consequences of restricting the angles of interaction by making the simple approximation of ignoring the ranges of translational energy. Thus in Fig. 9, we plot the velocity vectors corresponding to the most probable values for the $\mathbf{v}_K$ and $\mathbf{v}_{CH_3I}$ of Fig. 1. In Fig. 9a the vectors are arranged to correspond directly with the drawing of the apparatus in Fig. 2, while in Fig. 9b the vectors have been shifted to have a common origin. In the latter form the figure is called a Newton diagram (*18*) to emphasize that it provides a convenient summary of the restrictions imposed on the reaction by the requirement of the conservation of mass, energy, and momentum (the kinematics of the reaction). Scattering to an angle θ in the center-of-mass coordinate system produces a cone around the relative velocity (Fig. 9b). For a detector moving in the plane of $\mathbf{v}_{K}$ and $\mathbf{v}_{CH_3I}$ the same θ is obtained at two angles α_1 and α_2. Each different θ corresponds to two new values of α. The reason for the appearance of the cone is the independence of the scattering on the azimuthal angle ϕ which arises from the uniform distribution of incoming K in the plane perpendicular to **v** (Fig. 9d). The chance, therefore, of having a particular b is independent of ϕ. In Fig. 9c we show vectors for $\mathbf{v}_{KI}$ and $\mathbf{v}_{CH_3}$ forming cones about the same initial velocity **v**. This diagram is drawn to correspond to Fig. 8 (which shows the measured location of the maximum in the KI distribution at $\alpha = 83°$), making use of the fact that the spread of KI above and below the plane of $\mathbf{v}_{K}$ and $\mathbf{v}_{CH_3I}$ is very like that in the plane (*17*).

The center-of-mass vector is at an angle of $\sim 42°$ from $\mathbf{v}_{K}$ (diagrams in Fig. 9, a, b, and c). Thus, the observed KI distribution with its maximum near α equal to 83° is asymmetric with respect to the plane perpendicular to **v** at O′. The KI rebounds or returns to the direction from which the K originally came. We can conclude immediately that the lifetime of the complex K–I–CH_3 is comparable to (or shorter than) the time for one rotation of K–I–CH_3, about 10^{-13} second. A much longer lived complex would probably be equally likely to decompose in any phase of its rotation and thus give equal signals forward and backward along **v**. This is not a "sticky" collision, but a short interaction followed by the separation of products or of scattered reactants. Further, we can see that for KI molecules appearing at the peak of the distribution at $\alpha = 83°$, the KI and CH_3 separate with a speed v' of 13.7×10^4 cm/sec or a relative kinetic energy

$$E' = (1/2)\,\mu' v'^2 = 3.14 \text{ kcal/mole}$$

where μ' is the reduced mass of KI and CH_3. From the conservation of energy we have

$$E + E_{\text{int}} = E' + E'_{\text{int}} + \Delta E_0. \qquad (9)$$

E_{int} and E'_{int} are the sum of the rotational, vibrational, and electronic energies of the reactants and products respectively, and ΔE_0 is the energy change of the reaction at 0°K. From Fig. 1 we find $E \cong 1$ and $E_{\text{int}} \cong 0.5$ kcal/mole, so with our value of $E' = 3.14$ kcal/mole and an estimate $\Delta E_0 = -22$ kcal/mole we find $E'_{\text{int}} = 20$ kcal/mole. In other words, for KI mol-

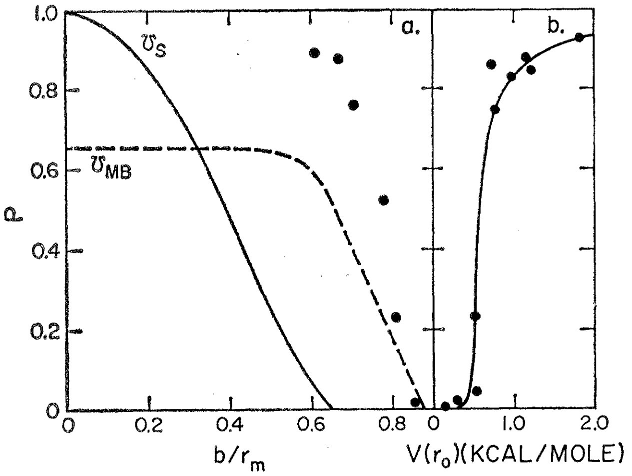

Fig. 6. The probability of reaction (a) versus impact parameter b and (b) plotted against potential energy at closest approach $V(r_0)$. The curves in (a) are obtained from the trajectory calculations of reference *24*.

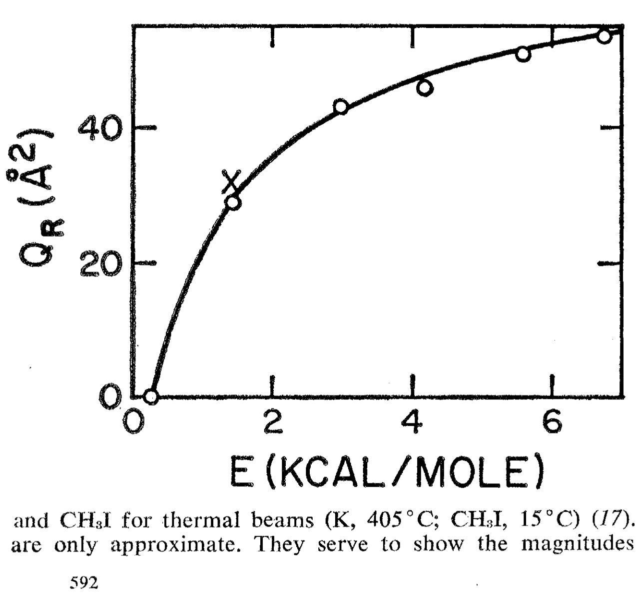

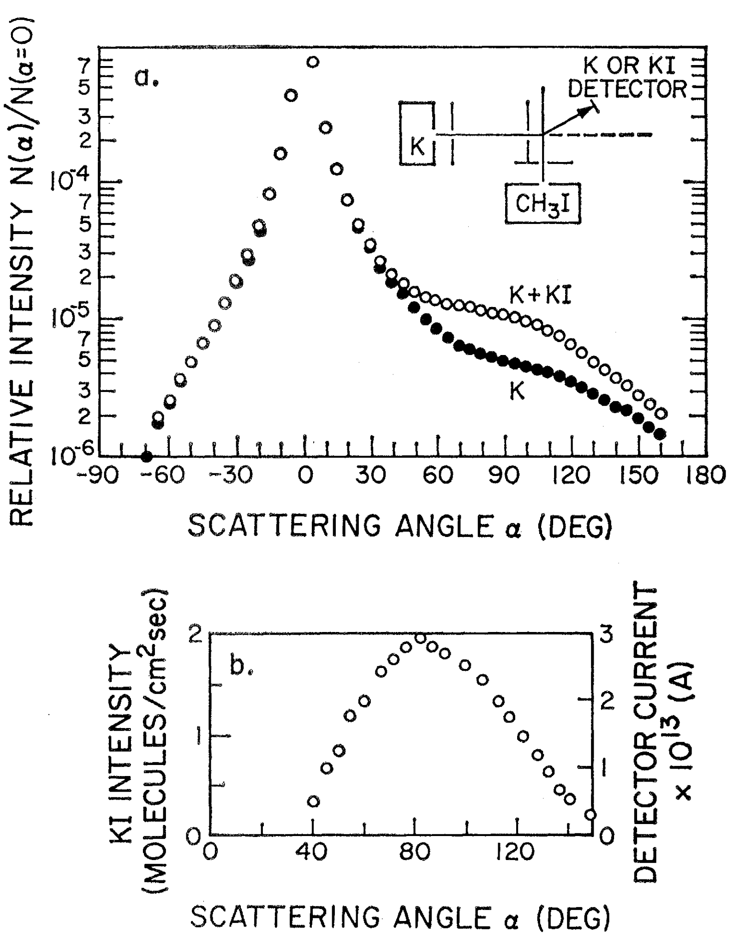

Fig. 7 (left). The total reaction cross section Q_R plotted against initial relative kinetic energy E; (○) from nonreactive scattering (*12*), (×) from reactive scattering (*17*). Fig. 8 (right). (a) Angular distribution of K and K + KI scattered after interaction of K and CH_3I for thermal beams (K, 405°C; CH_3I, 15°C) (*17*). (b) Angular distribution of KI (*17*). The absolute values on the ordinates are only approximate. They serve to show the magnitudes of the quantities.

ecules detected at $\alpha = 83°$, nearly 90 percent of the available energy appears as rotational and vibrational energy of the products; these species are not blown apart rapidly, but separate from each other with a relatively small speed.

Although the peak of the KI distribution would seem to represent the most likely result of a reactive collision, a more detailed analysis (*17*) shows that KI molecules with v' greater than 13.7×10^4 cm/sec are actually produced more frequently than are those which appear at $\alpha = 83°$. The observed laboratory distribution is a seriously distorted version of the distribution in the center-of-mass coordinate system. The most probable E' turns out to be about 13 kcal/mole, so the corresponding E'_{int} is about 10 kcal/mole. The amount of internal energy in the products has been determined more directly for other exothermic reactions from measurement of the velocity of one product by means of another set of rotating slotted discs, a velocity analyzer (*19*). This discussion of the anisotropy of the distribution of products is based, of course, on the simplification of using a single Newton diagram, that is, a single energy E and a single direction of relative motion $\mathbf{v}$.

One more result can be derived from results like those shown in Fig. 8. By adding up the KI for the whole range of α (including that KI which appears above and below the plane of the two beams) for given intensities of K and CH_3I, Hershbach, Kwei, and Norris (*17*) found that the total reaction cross section is $Q_R \cong 30$ Å^2. The agreement of this value with the one derived from the elastic scattering is all that can be asked, because either one can be reasonably expected to be in error by as much as a factor of 2.

Recently, Brooks and Jones, and Beuhler, Bernstein, and Kramer (*20*) have refined the experiment of Herschbach, Kwei, and Norris (*17*); these groups used beams of CH_3I in which the molecules were oriented so that the alkali atom could be made to approach the CH_3I principally either from the I end or, with the opposite setting of the polarizer, from the CH_3 end. The orientation was achieved in a six-pole electric field (*21*) which gave degrees of alignment approximately as indicated in Fig. 1h. The results show that the ratio of the reaction cross sections for the potassium approaching CH_3I from the I and CH_3 ends is substantially greater than 1 ($\approx$ 1.5). This is, of course, just what most chemists would expect. The experiment is a new, quantitative approach to measuring the elusive steric factor which has long served to summarize ignorance of orientation requirements for reactions.

Theoretical Studies

Up to this point we describe what molecular-beam experiments have told about the reaction of potassium and methyl iodide; now we compare these results with others from theoretical work on this reaction. The complete quantum mechanical treatment of such a complicated system as this one is still

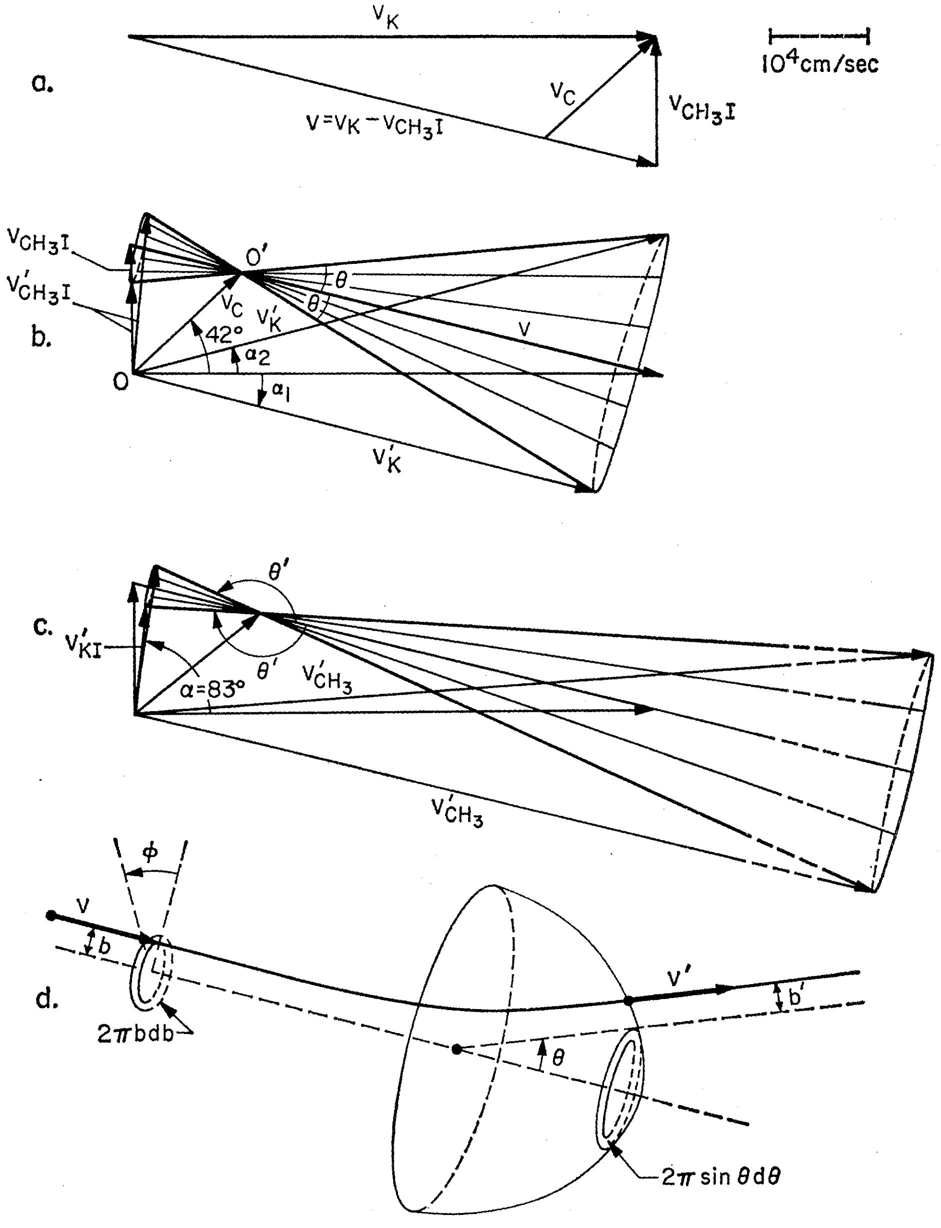

Fig. 9. (a–c) Velocity vector diagrams for beams of K and CH_3I intersecting at 90°. The lengths of the vectors correspond to the most probable velocities of Figs. 1 and 8. Laboratory velocity of species i before (after) collision $\mathbf{v}_i(\mathbf{v}'_i)$; relative velocity before (after) collision $\mathbf{v}(\mathbf{v}')$. (a) Vectors arranged to match the apparatus drawing in Fig. 2. (b) Vectors $\mathbf{v}_K$, $\mathbf{v}_{CH_3I}$ shifted to a common origin O. Cone shows elastic scattering of K to angle θ from $\mathbf{v}$. (c) Cone for reactive scattering of KI to θ' about $\mathbf{v}$. The cone for $\mathbf{v}'_{CH_3}$ has been distorted by shortening it to 0.6 of its correct height. (d) Uniform distribution of trajectories (independent of ϕ) produces uniform scattering in a cone around $\mathbf{v}$. The initial and final impact parameters are b and b'. The hemisphere is drawn in only to emphasize the spherical coordinate system convenient for the final relative velocity $\mathbf{v}'$.

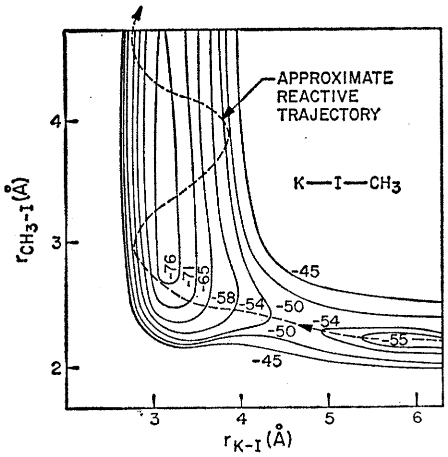

Fig. 10. Potential energy surface $\mathcal{V}_{\mathrm{MB}}$ of reference (*23, 24*) for linear configuaration K-I-CH$_3$. Contours show energies in kilocalories per mole referred to zero for both $r_{\mathrm{K-I}}$ and $r_{\mathrm{I-CH_3}}$ large. Dashed line shows an approximate trajectory for a reactive collision.

entirely out of the question. However, progress is being made in a number of directions. Some studies on classical trajectories are discussed here.

Blais and Bunker, and Raff and Karplus (*22–24*) have made the assumption that classical mechanics is sufficient to describe the important characteristics of a reactive collision once the forces between all the atoms are known. They reduce the problem to an interaction of three bodies by taking the methyl group as a single particle of mass 15 atomic mass units. Figure 10 shows one of the potential energy surfaces ($\mathcal{V}$) Raff and Karplus used. The contour lines connect points of equal potential energy for a linear collision in which K approaches CH$_3$I from the I end. This is a simplified representation; the calculations are not restricted to linear collisions.

For the latter, more general situation the surface must be represented by a series of diagrams like Fig. 10, one for each CH$_3$–I–K angle. A reactive collision is represented by a point moving on this surface from the lower right to the upper left. The dashed line shows one possible path or trajectory for the surface of Fig. 10. This trajectory rises from the valley it starts in (at the lower right) to cross through the pass and then to descend to the valley leading to the top of the page. The oscillations in this part of the trajectory show the vibration of the new KI molecule. For a nonreactive collision, a trajectory approaches the pass as before but, instead of crossing through, turns about and leaves from the valley where it entered.

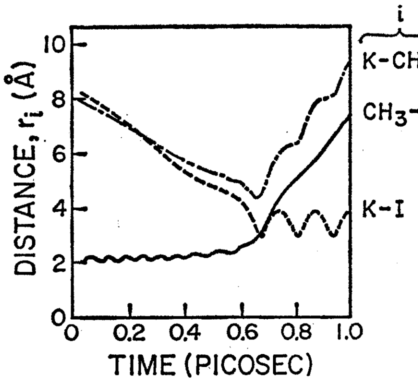

Fig. 11. Variation with time of internuclear distances for a reactive collision. CH$_3$I is rotating as K approaches, but KI leaves with little rotational energy (*23*).

An alternative representation, which is not restricted to showing only one configuration for the three particles, is to plot the values for the three internuclear distances against time. Figure 11 shows a reactive collision in this representation. From observing that the sum $r_{\mathrm{K-I}}$ and $r_{\mathrm{CH_3-I}}$ is appreciably greater than $r_{\mathrm{K-CH_3}}$ before the collision at 0.6×10^{-12} second on this diagram, we can see that this collision is not even nearly a linear one. In representing a real system by a set of trajectories, Raff and Karplus take care to select the latter (characterized by v, b, J, V, and γ) appropriately to correspond to the actual distributions of the reactants. These distributions may be thermal ones with given T_{K} and $T_{\mathrm{CH_3I}}$, like those indicated in Fig. 1, or selected in an arbitrary way.

These calculations are useful for exploring how changes in the potential surface affect the partition of energy between translation, rotation, and vibration of the products, the laboratory angles at which the products are concentrated, and the variation of the probability of reaction with E, b, and the threshold potential energy $V(r_0)$. Curves for the two latter quantities $P(b)$ and $P(V(r_0))$ are shown for two potential energy surfaces in Fig. 6 together with the points obtained from the measurements of the nonreactive scattering. The essential difference between these two surfaces is that $\mathcal{V}_{\mathrm{MB}}$ contains a term to provide repulsion between CH$_3$ and K which makes the reaction cross section depend significantly on the orientation of the CH$_3$I. The surface $\mathcal{V}_{\mathrm{S}}$ is much more nearly spherically symmetrical. Both surfaces give curves in fair agreement with the points in Fig. 6, a result which may indicate that the surfaces are realistic ones. The two surfaces give similar predictions for most properties of the reaction such as the ratio of the energy in internal excitation to that of relative translational motion for the products ($E'_{\mathrm{int}}/E' \cong 6$ for $\mathcal{V}_{\mathrm{MB}}$ and $\cong 3$ for $\mathcal{V}_{\mathrm{S}}$) and the total reaction cross section ($Q_R = 25$ Å^2 for $\mathcal{V}_{\mathrm{MB}}$ and $= 13$ Å^2 for $\mathcal{V}_{\mathrm{S}}$, almost independent of the initial relative speed v). These predictions compare with the experimental results (*2, 15*) that $E'_{\mathrm{int}}/E' = 7$ and $Q_R = 30$ Å^2 at $E = 2$ kcal/mole. The reinterpretation (*17*) mentioned above only changes E'_{int}/E' which now becomes 0.5. (This new value was not available when Raff and Karplus did their work.) The choice of a surface which gives $E'_{\mathrm{int}}/E' = 1$ leads to a long-lived complex CH$_3$–I–K in disagreement with the interpretation of the experimental results, a lifetime of less than one rotation time. As Karplus and Godfrey (*25*) show, one reason for preferring $\mathcal{V}_{\mathrm{MB}}$ over $\mathcal{V}_{\mathrm{S}}$ is that the former succeeds, while the latter fails, in predicting the observed variation of the reaction cross section with the orientation of CH$_3$I toward K. This is an example of how comparison of the experimental results and the calculations leads to knowledge of the potential energy surface for the reaction.

Finally, we note that a calculation of the effective two-body potential for elastic scattering (the optical potential) for a surface of the kind used in reference *24* is in reasonable agreement with the repulsive potential deduced from the measurements on elastic scattering (*26*).

Conclusion

Molecular-beam experiments, the interpretation of these experiments, and theoretical studies of reactive collisions are bringing new information to chemical kinetics. For our sample reaction we can now list values for such detailed quantities as the total cross section; parameters for the interaction potential for the reactants; the threshold energy, distance, and impact parameter; the probability of reaction as it varies with b and $V(r_0)$; the reaction cross section as it varies with energy and orientation; and the partitioning of energy between the internal and translational energy of the products. This is a start in looking inside the thermal distributions of kinetics to discover more about what happens in reactive collisions.

References and Notes

1. T. H. Bull and P. B. Moon, *Disc. Faraday Soc.* **17**, 54 (1954); E. H. Taylor and S. Datz, *J. Chem. Phys.* **23**, 1711 (1955).
2. D. R. Herschbach, *Advances Chem. Phys.* **10**, 319 (1966).
3. E. F. Greene, A. L. Moursund, J. Ross, *ibid.*, p. 135.
4. A. R. Blythe, M. A. D. Fluendy, K. P. Lawley, *Quart. Rev. (London)* **20**, 465 (1966); J. P. Toennies, in *Elementary Processes and Chemical Reactions*, H. Hartmann and J. Heidberg, Eds. (Springer Verlag, Heidelberg, 1967); R. B. Bernstein, *Science* **144**, 141 (1964).
5. M. Polanyi, *Atomic Reactions* (Williams and Northgate, London, 1932).
6. H. von Hartel and M. Polanyi, *Z. Physik. Chem. Ser. B* **11**, 97 (1931).
7. E. W. Rothe and R. B. Bernstein, *J. Chem. Phys.* **31**, 1619 (1959).
8. E. W. Rothe and R. H. Neynaber, *ibid.* **43**, 4177 (1965).
9. E. A. Gislason and G. H. Kwei, *ibid.* **46**, 2838 (1967).
10. R. B. Bernstein and K. H. Kramer, *ibid.* **38**, 2507 (1963).
11. At very large r, retardation effects become important, and the potential varies as r^{-7} [P. R. Fontana and R. B. Bernstein, *ibid.* **41**, 1431 (1964)].
12. J. R. Airey, E. F. Greene, G. P. Reck, J. Ross, *ibid.* **46**, 3295 (1967).
13. F. T. Smith, R. P. Marchi, K. G. Dedrick, *Phys. Rev.* **150**, 79 (1966).
14. R. M. Eisberg and C. E. Porter, *Rev. Mod. Phys.* **33**, 190 (1961); D. Beck, E. F. Greene, J. Ross, *J. Chem. Phys.* **37**, 2895 (1962); J. L. J. Rosenfeld and J. Ross, *ibid.* **44**, 188 (1966).
15. D. R. Herschbach, G. H. Kwei, J. A. Norris, *J. Chem. Phys.* **34**, 1842 (1961).
16. Any suggestion that the KI signal may have been K atoms somehow misidentified was resolved by an experiment in which a magnetic deflecting field was used to remove any paramagnetic atoms while permitting the nonmagnetic KI molecules to pass unhindered, R. R. Herm, R. Gordon, D. R. Herschbach, *ibid.* **41**, 2218 (1964).
17. G. H. Kwei, J. A. Norris, J. L. Kinsey, D. R. Herschbach, in preparation.
18. D. R. Herschbach, *Disc. Faraday Soc.* **33**, 149 (1962).
19. A. E. Grosser and R. B. Bernstein, *J. Chem. Phys.* **43**, 1140 (1965); J. H. Birely and D. R. Herschbach, *ibid.* **44**, 1690 (1966).
20. P. R. Brooks and E. M. Jones, *ibid.* **45**, 3449 (1966); R. J. Beuhler, J., R. B. Bernstein, K. H. Kramer, *J. Amer. Chem. Soc.* **88**, 5331 (1966).
21. K. H. Kramer and R. B. Bernstein, *J. Chem. Phys.* **42**, 767 (1965).
22. N. C. Blais and D. L. Bunker, *ibid.* **37**, 2713 (1962); **39**, 315 (1963).
23. M. Karplus and L. M. Raff, *ibid.* **41**, 1267 (1964).
24. L. M. Raff and M. Karplus, *ibid.* **44**, 1212 (1966). For review see M. Karplus, in *Structural Chemistry and Molecular Biology*, A. Rich and N. Davidson, Eds. (Freeman, San Francisco, 1967).
25. M. Karplus and M. Godfrey, *J. Amer. Chem. Soc.* **88**, 5332 (1966).
26. B. C. Eu and J. Ross, *Disc. Faraday Soc.*, in press.
27. Supported in part by AEC and NSF. We thank D. R. Herschbach, J. L. Kinsey, G. H. Kwei, and J. A. Norris for allowing the use of their recent work before its publication; R. B. Bernstein, D. R. Herschbach, and A. Persky for reading the manuscript; and the members of the chemistry department of the California Institute of Technology, particularly Prof. A. Kuppermann, for hospitality to E.F.G.

The Role of Systematics in Biology

The study of all aspects of the diversity of life is one of the most important concerns in biology.

Ernst Mayr

There are many ways of dealing with the topic that was assigned to me. One might give a history of the role which taxonomy has played in the development of biology; or one might concentrate on the present status of systematics in biology; or finally one might attempt, in a timeless and somewhat philosophical way, to delineate the niche which systematics occupies within the total conceptual framework of biology. Further thought makes it evident that the three approaches are interdependent to such a degree that one has to give due consideration to all three of them.

Let me start with the question, what do we mean by "systematics," the role of which I am to describe? To be able to answer this question meaningfully requires an excursion into the history as well as philosophy of biology. The ancient Greeks saw a natural order in the world which, they thought, could be demonstrated and classified by certain logical procedures. They tried to discover the true nature of things (their essences) and approached classification with the methods of logic. Indeed, Aristotle, the first great classifier, was also the father of logic. The underlying philosophy, now usually referred to as essentialism (from essence), dominated the thinking of taxonomists up to and including the time of Linnaeus. Taxonomic nomenclature and the so-called typological thinking of taxonomists right up to our day have been permanently affected by the Aristotelian heritage (*1*).

History of Taxonomy

During the early history of biology this was no great handicap. Botany and zoology, to state it in a highly oversimplified manner, arose from the 16th century on as applied sciences, attached to medicine. Botany started as a broadened study of medicinal herbs and early botanical gardens were herb gardens. With but one or two exceptions all the great botanists and herbalists from the 16th to the 18th century (Linnaeus included) were professors of medicine or practicing physicians. Zoology arose in connection with human anatomy and physiology. When botany and zoology became independent sciences, the first concern of the two fields was to bring order into the diversity of nature. Taxonomy was therefore their dominant concern, and indeed in the 18th and early 19th century botany and zoology were virtually coextensive with taxonomy. Moreover, by sheer necessity, taxonomy was essentially the technique of identification.

The middle third of the 19th century was a period of decisive change to which many separate streams of development contributed. Increasing professionalism was one, and increasing specialization was another, to mention just two. Taxonomy itself helped in accelerating the change by introducing several new concepts into biology. The greatest unifying theory in biology, the theory of evolution, was largely a contribution made by the students of diversity, as we might call the taxonomists. It is no coincidence that Darwin wrote his *Origin of Species* after encountering taxonomic problems dur-

---

The author is Alexander Agassiz Professor of Zoology and Director of the Museum of Comparative Zoology at Harvard University, Cambridge, Massachusetts. This article is based on an invitation lecture presented at the International Systematics Conference at Ann Arbor, Michigan, 14–16 June 1967. A volume of the contributions to this conference is now in press (National Research Council).